symmetry

MDPI

Article

Structure Determination Feasibility of Three-Dimensional Electron Diffraction in Case of Limited Data

Partha Pratim Das [1,†], Sergi Plana-Ruiz [1,2,†], Athanassios S. Galanis [1], Andrew Stewart [3,*], Fotini Karavasili [4], Stavros Nicolopoulos [1,*], Holger Putz [5], Irene Margiolaki [4], Maria Calamiotou [6] and Gianluca Iezzi [7,8]

1 NanoMEGAS SPRL, Rue Èmile Claus 49 bte 9, 1050 Brussels, Belgium
2 Servei de Recursos Científics i Tècnics, Universitat Rovira i Virgili, Avinguda dels Països Catalans 26, 43007 Tarragona, Catalonia, Spain
3 Department of Chemistry, University College London, London WC1H 0AJ, UK
4 Section of Genetics, Cell Biology and Development, Department of Biology, University of Patras, GR-26500 Patras, Greece
5 CRYSTAL IMPACT, Dr. H. Putz & Dr. K. Brandenburg GbR, 53227 Bonn, Germany
6 Section of Condensed Matter Physics, Physics Department, University of Athens, GR-15784 Athens, Greece
7 Dipartimento di Ingegneria & Geologia (INGEO), University G. d'Annunzio of Chieti-Pescara, Via Dei Vestini 30, 66100 Chieti, Italy
8 INGV (Istituto Nazionale di Geofisica e Vulcanologia) Roma, Via di Vigna Murata 605, 00143 Roma, Italy
* Correspondence: andy.stewart@ucl.ac.uk (A.S.); info@nanomegas.com (S.N.)
† These authors contributed equally to this work.

check for updates

Citation: Das, P.P.; Plana-Ruiz, S.; Galanis, A.S.; Stewart, A.; Karavasili, F.; Nicolopoulos, S.; Putz, H.; Margiolaki, I.; Calamiotou, M.; Iezzi, G. Structure Determination Feasibility of Three-Dimensional Electron Diffraction in Case of Limited Data. *Symmetry* **2022**, *14*, 2355. https://doi.org/10.3390/sym14112355

Academic Editor: Vasilis K. Oikonomou

Received: 4 October 2022
Accepted: 28 October 2022
Published: 8 November 2022

Abstract: During the last two decades, three-dimensional electron diffraction (3D ED) has undergone a renaissance, starting with the introduction of precession (Precession Electron Diffraction Tomography, PEDT) that led to variations on the idea of collecting as much of the diffraction space as possible in order to solve crystal structures from sub-micron sized crystals. The most popular of these acquisition methods is based on the continuous tilting/rotation of the crystal (so-called Microcrystal Electron Diffraction, MicroED) akin to the oscillating crystal method in X-ray crystallography, which was enabled by the increase of sensitivity and acquisition speed in electron detectors. While 3D ED data is more complex than the equivalent X-ray data due to the higher proportion of dynamical scattering, the same basic principles of what is required in terms of data quality and quantity in order to solve a crystal structure apply; high completeness, high data resolution and good signal-to-noise statistics on measured reflection intensities. However, it may not always be possible to collect data in these optimum conditions, the most common limitations being the tilt range of the goniometer stage, often due to a small pole piece gap or the use of a non-tomography holder, or the position of the sample on the TEM grid, which may be too close to a grid bar and then the specimen of interest becomes occluded during tilting. Other factors that can limit the quality of the acquired data include the limited dynamic range of the detector, which can result on truncated intensities, or the sensitivity of the crystal to the electron beam, whereby the crystallinity of the particle is changing under the illumination of the beam. This limits the quality and quantity of the measured intensities and makes structure analysis of such data challenging. Under these circumstances, traditional approaches may fail to elucidate crystal structures, and global optimization methods may be used here as an alternative powerful tool. In this context, this work presents a systematic study on the application of a global optimization method to crystal structure determination from 3D ED data. The results are compared with known structure models and crystal phases obtained from traditional ab initio structure solution methods demonstrating how this strategy can be reliably applied to the analysis of partially complete 3D ED data.

Keywords: 3D ED; MicroED; precession electron diffraction; crystal structure determination; global optimization methods

1. Introduction

Structure solution of crystalline materials via electron diffraction (ED) methods has a long history stretching back several decades [1–4]. While the technique has an obvious appeal of being able to solve structures from the smallest of crystals, it was not widely adopted owing to major challenges with data collection and analysis. In fact, it was initially believed that only zone axis diffraction patterns with the corresponding image was the only method to overcome the interpretation of highly dynamical zone axis data, a very slow and technically challenging process [5]. The inherent dynamical diffraction effects present in ED data are due to the $10^{3–4}$ stronger interactions of electrons with respect to X-rays, a feature that allows to focus an electron beam to few nanometres but increases the likelihood of multiple scattering events [6–8].

Direct methods were one of the initially available algorithms for crystal structure determination that were developed for X-ray diffraction data. This means that the kinematic theory of diffraction was assumed to process the reflection intensities, i.e., a single scattering event for each photon interacting with a crystal. Nevertheless, direct methods are based on statistical distributions that makes them more robust to noise than other approaches, such as charge-flipping, which uses the measured intensities directly to reconstruct the crystal phase. This can be seen in the fact that direct methods were developed in an era when intensities were being measured by eye and categorised into a series of intensity bins, from strong to weak. However, ED patterns only from zone axes are too dynamical even for the robustness of direct methods [9].

The key advantage of structure analysis by using a transmission electron microscope (TEM) is the ability to probe and extract information from nanometre-sized volumes of individual crystals/materials, which is often challenging or impossible via traditional single-crystal X-ray diffraction methods available in most structural analysis laboratories. It was not until the development of precession electron diffraction (PED) by Vincent and Midgley [10], and Own [11], as well as the commercial availability of a precession-signal generator (SpinningSTAR, DigiSTAR from NanoMEGAS SPRL) [12,13], that ED took a major step forward on the analysis of nanocrystals [12]. PED leads to higher number of reflections in a diffraction pattern, better integration of reflection intensities and reduced dynamical effects. Besides structure solution, PED has also been proved to be advantageous for phase and orientation mapping [14], strain analysis [15] and electron pair distribution study of nanoparticles [16].

PED demonstrated that collecting data away from the perfectly aligned zone axis was advantageous by significantly reducing the dynamical diffraction effects due to the integration of the reflection intensities [10]. This initial idea was then extended by Ute Kolb's group, which introduced the sequential acquisition of PED patterns from a random crystal orientation without the need to find the different zone-axes, further reducing the dynamical effects, and obtaining a quasi-kinematic ED dataset that enabled direct methods to be robust enough to solve structures ab initio. The data acquisition was achieved by combining PED and the acquisition methodology of image tomography, demonstrating for the first time an efficient method for collecting three-dimensional electron diffraction (3D ED) data, an acquisition routine also known as Precession Electron Diffraction Tomography (PEDT) [17–21]. This is performed by tilting the crystal in 1° increments around the tilt axis of the TEM goniometric stage and recording a diffraction pattern with a precessed beam for each tilt. A precession angle of 1° is usually used to ensure that the diffraction space is integrated ~ ±1° around the stage position, integrating the Bragg reflections on an electron detector in a manner analogous to the X-ray oscillating crystal method (Figure 1). Data processing is then followed by different available software, e.g., ADT3D [17,18] distributed by Nanomegas SPRL [13], RED [22,23] or PETS2 [24], that have been specifically developed to determine unit cell parameters and extract the recorded reflection intensities from 3D ED data. The extracted intensities are subsequently used for structure solution using either direct methods as implemented in SIR software [25–27] or charge-flipping as implemented in Jana 2006 [28,29]. In recent years, the development of CMOS-based detectors for indirect (optical

fibre coupled) and direct electron detection [30,31] have enabled the collection of ED data by continuously rotating the crystal [32,33], a method known as MicroED (Microcrystal Electron Diffraction) [34], thus increasing the easiness to acquire such kind of datasets. With the rapid advances of 3D ED methods, many X-ray crystallography software packages (e.g., XDS, DIALS) [35,36] have also been adapted to process 3D ED data, further lowering the barrier for X-ray crystallographers to familiarise with ED techniques.

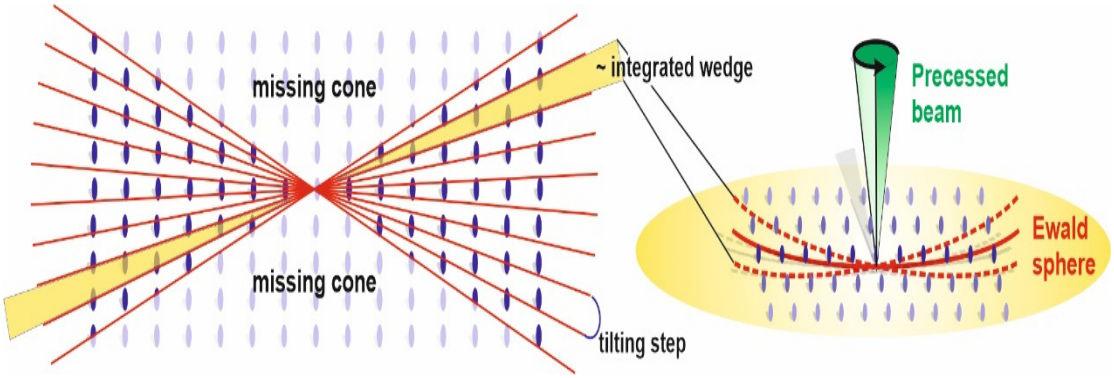

Figure 1. Illustration of the data collection procedure viewed along the tilt axis (**left**) and the use of beam precession to integrate reflections along the excitation error (**right**).

Direct methods and charge-flipping require high data completeness for successful and reliable structure determination [37–40]. The continuous rotation approach depends on the accessibility of modern CMOS-based detectors as well as holders and stages of large tilt range capabilities. Direct electron cameras like hybrid-pixel detectors are more sensitive and can detect electrons more efficiently than charge-coupled devices (CCD's). In addition, hybrid-pixel detectors have a significantly faster readout mechanism, which enables the collection of the continually rotating crystal with minimal to no loss of data in the recorded integrated volume. The higher sensitivity of this technology enables beam sensitive materials to be collected at very low dose conditions that would not be possible with a CCD [32]. In circumstances where only a CCD is available, acquiring sufficient high-quality diffraction data from beam sensitive materials at room temperature is challenging or, in some cases, impossible to allow a successful ab initio crystal structure determination. In this situation of low data completeness and/or low resolution, an alternative approach for crystal structure determination is to apply global optimization methods, since they have been shown to be a particular powerful tool for the retrieval of crystal phases from powder X-ray diffraction data [41,42].

Global optimization is a numerical analysis method attempting to find a global minimum or maximum of a so-called "cost function" (which in turn can be a combination of functions on a given set of variables, here the crystal structure data). Global optimization methods have been extensively used for solving molecular and ionic structures from powder X-ray diffraction [26,42–51] as well as from ED data [52–54]. This approach requires generating initial structure models either at random or based on the known molecular connectivity for organics or known polyhedral geometry for inorganic compounds [55–57]. In global optimization methods, the positions of individual atoms as well as the global shift and rotation of the molecule and non-constrained torsional angles are free to vary until an optimal agreement between the observed and calculated reflection intensities is obtained. Depending on the complexity of the problem, different global optimization techniques such as Monte Carlo, simulated annealing or genetic algorithms can be employed for structure analysis [58].

In this work, we present the study of 3D ED data of limited quality and resolution from four different inorganic crystalline materials to evaluate the feasibility of successful crystal structure determination. First, the traditional ab initio approaches of direct methods and charge-flipping are used to find and understand the limitations of low-quality data.

Then, the obtained structure models are compared to the ones determined from the global optimization method to show how it can be used as an additional and helpful tool for crystal structure analysis when only limited or constrained data is available.

2. Materials and Methods

2.1. Materials

Four different known inorganic materials have been studied by means of 3D ED: $PrBa_2Cu_3O_7$, $BaCuO_2$, $LiAl_{0.8}Fe_{0.2}(SiO_3)_2$ and $LiAl(SiO_3)_2$. $PrBa_2Cu_3O_7$ is the well-known Pr123 material that lacks the superconductivity properties of the Y123-type materials [59,60], while $BaCuO_2$ is always present as an impurity in the Pr123 samples due to antisite defects (Ba atom on Pr site for Pr123 compound), which has also been previously detected by powder diffraction [60,61]. $LiAl(SiO_3)_2$ (spodumene) is a pyroxene mineral, a single-chain silicate (inosilicate), that is an important source of lithium for ceramics, mobile phones and automotive batteries [62]. $LiAl_{0.8}Fe_{0.2}(SiO_3)_2$ is also an inosilicate from the spodumene family in which the aluminum position has been partially occupied by iron [63–65]. From a crystallographic point of view, Pr123 grows in an orthorhombic crystal system with space group *Pmmm* and lattice parameters a = 3.8605 Å, b = 3.9243 Å and c = 11.6993 Å [60,66]. $BaCuO_2$ is a cubic crystal in the $I\,m\bar{3}m$ space group with a = 18.2700 Å [67], and both lithium-ion compounds are monoclinic crystals with space group $C\,2/c$ and the following lattice parameters: a = 9.474 Å, b = 8.390 Å, c = 5.219 Å and β = 110.07° for $LiAl(SiO_3)_2$ [60,62], and a = 9.490 Å, b = 8.426 Å, c = 5.232 Å and β = 110.14° for $LiAl_{0.8}Fe_{0.2}(SiO_3)_2$ [65].

2.2. 3D ED Acquisitions

Samples for TEM measurements were prepared by crushing the raw material with a mortar and pestle to a fine powder. Then, the specimen was dispersed on a 200 mesh Cu-TEM grid with a continuous amorphous carbon film.

3D ED data were collected with a JEOL 2100 LaB_6 TEM operated at 200 kV in TEM mode with a standard single-tilt JEOL holder, and equipped with a precession signal generator (SpinningStar, provided by Nanomegas) [13]. A side-entry Gatan ES500W camera was used for the acquisition of the diffraction data, which is a CCD detector that views a fluorescent screen tilted 45° with respect to the horizontal plane of the TEM. This detector was one of the first CCD's available for the TEM market and has a low dynamic range (12-bit) as well as low sensitivity compared to more modern CCDs. However, it has been proved that such kind of experimental setup can be used for structure solution and even structure refinements based on the kinematic and even dynamical theory of diffraction in some cases [68,69]. Nevertheless, the dataset of $LiAl(SiO_3)_2$ was acquired with a post-column Gatan UltraScan1000 CCD camera (16-bit) placed on a FEI Tecnai F30 TEM operated at 300 kV in STEM mode for quality comparisons.

Diffraction data were acquired in selected-area electron diffraction mode using a 50-µm selected-area aperture, a 70-µm condenser aperture, and a quasi-parallel beam obtained by spreading the beam across a large area [20,70]. Crystals of around 400 nm in size were selected in imaging mode and the thin edges of the crystals were utilised. Although automatic procedures for this kind of experiments are available nowadays [69,71], diffraction data was collected following a manual procedure. Each targeted crystal was standing at an arbitrary crystallographic axis orientation and diffraction patterns were acquired by tilting the holder between −30° and +30° with a tilt step of 1° (maximum available tilt range according to the used pole pieces and single-tilt holders), consequently recording 61 diffraction patterns. Each diffraction pattern was recorded with a precession angle of 1°, the exception being $BaCuO_2$, where precession was not used to compare results between PED and non-PED data. The tilting of the goniometric stage was controlled by a Digital Micrograph script to ensure that each tilt step corresponded to 1°, which included a feedback loop in the form of a *while* and *if* statements to ensure that the requested tilt angle was obtained with an error of less than 0.05°. Crystal tracking was achieved by defocusing the central beam of the diffraction pattern, whereby it is possible to visualize the crystal

as a shadow image inside the zero order (non-diffracted) beam of the pattern, correcting the crystal movement by the x and y shifts of the stage, and refocusing it to collect the subsequent precessed diffraction pattern.

The ADT3D software (also called eADT [13,72,73]) was used to process the acquired dataset. This software merges the recorded diffraction patterns into a 3D reconstruction of the diffraction space accounting for pattern shifts that occur during the acquisition process. The software then determines the unit cell parameters, indexes the reflections, and extracts the intensity of the indexed reflections to produce a *hkl* file ready for crystal structure determination. Datasets with precession were also processed with PETS2 in order to analyse the double-peaked rocking curves caused by the reflection integration of the precession movement [24].

2.3. Structure Determination Tools

Direct Methods & Charge-Flipping

Ab initio crystal structure solutions were obtained via direct methods and the charge-flipping procedure with the *hkl* files obtained from ADT3D and PETS2. Direct methods from the SIR2014 software package with the appropriate ED settings and the charge-flipping implemented in SUPERFLIP inside the Jana 2006 software suite were used to solve the crystal structures [28,74–76].

2.4. Global Optimization Method

In contrast to direct methods, a reciprocal space method, and charge-flipping, an iterative dual space method, the global optimization method typically uses the so-called "direct-space" approach [45–49]. This means that a complete structure model (including unit cell parameters, space group and atomic positions) is proposed at first independently of the diffraction information [46–48,77,78]. Afterwards, this model is repeatedly varied and evaluated by comparing its calculated diffraction pattern to the experimental one. The goal is to reduce the so-called "cost function" (e.g., difference between calculated and experimental diffraction pattern) as far as possible until the global minimum is reached (in the optimal case). If no other constraints are introduced, this straightforward prescription, also known as the "Reverse Monte Carlo"-method [79,80], is limited in practice by the fact that for most crystalline solids the system is quickly trapped in a minimum that does not correspond to a physically reasonable atomic arrangement. The reason for this lies in the landscape of the cost function which includes numerous deep local minima [80]. To resolve (or at least reduce) this problem, prior chemically reasonable knowledge about the crystal structures, like sensible interatomic distances, connectivity (molecules) or atomic charges (ions), can be readily applied with the direct-space approach during the structure solution calculation. For example, in case of molecular structures, the structure solution calculation can be reduced to the determination of the 3-dimensional rotation and bond angles as well as the location of the molecule within the unit cell.

In this study we use the global optimization method as it is implemented in the Endeavour software [50,51]. Endeavour solves crystal structures by applying a combined global optimization of the differences between the calculated and the measured diffraction patterns (evaluated by the R factor) and, at the same time, the potential energy of the system ("Pareto-optimization" [81]) to avoid the aforementioned traps.

Each part of the cost function (potential energy and pattern difference) depends on all atomic coordinates, thus setting up a high dimensional hypersurface. "Merging" both hypersurfaces weakens or even eliminates the minima that belong to only one of the two surfaces and strengthens those which belong to both. Therefore, a sufficiently long global optimization run should sooner or later reach the global minimum of the system corresponding to the correct crystal structure.

In principle, any method for the calculation of the potential energy can be used, but the global optimization often makes ab initio energy calculations not feasible. Ab initio energy calculations have two drawbacks in this context. First, they are relatively time-consuming

compared to energy calculations using empirically derived potential functions, while typical Endeavour runs require millions of energy calculations in a reasonable amount of time. Second, although they work quite well in equilibrium states, there is always a certain risk that no convergence can be reached for chemically/physically "unreasonable" atomic arrangements where the common wave functions and approximations may no longer be applicable. Both drawbacks are not favorable for a routine application of the method, especially if non-expert users are involved. Fortunately, it turns out that at least for inorganic compounds that can be described with ions, a combination of the corresponding Coulomb forces [82] and a simple repulsion potential parametrized by minimum interatomic distances is generally sufficient.

In order to find the global minimum of the hypersurface, Endeavour uses "simulated annealing", a Monte Carlo-based global optimization method [83]. The idea of "simulated annealing" is to randomly walk around the hypersurface of the cost function(s), controlled by an algorithm that does not only walk "downhill" but also accepts modifications that cause an increase of the cost function with a certain probability (controlled by the "temperature" parameter). In the beginning of the optimization (structure solution calculation), the "temperature" value (i.e., the control parameter) is rather high, so that the probability that "bad" modifications are accepted is large and the system can walk around and visit large parts of the hypersurface of the cost function(s). When the calculation progresses, the "temperature" is reduced more and more, so that the probability to accept "bad" modifications is decreased. Therefore, the system will most probably be getting trapped in the deepest minimum (with regard to the number of states), which is supposed to be coincident with the deepest (hopefully global) minimum of the hypersurface.

In practice, it turns out that despite the inclusion of the potential energy during the structure solution process the hypersurface created by the two cost function contributions (*R* factor and potential energy) can still be rough and difficult to optimize. This is especially true if space groups with many different special positions and/or high multiplicities of the general or special positions are used, or diffraction data is of low quality (beam damage, dynamical diffraction effects, low completeness, missing high resolution reflections, poor signal-to-noise ratio, etc.). For structures with different special positions or high multiplicities, a small coordinate change of one atom on a special position with high multiplicity may change the entire structure, thus it may also significantly vary the *R* factor due to the number of atoms in the unit cell that are involved. To converge the solution, more weight is usually given to the long-range Coulomb potential energy instead of the contribution from the diffraction data (*R* factor), otherwise the correct atoms positions are challenging to obtain.

For crystal structures with larger unit cells and numbers of atoms, the number of possible atomic positions in the unit cell (possible configurations) increases exponentially. This causes an exponential increase of computing time for any global optimization method. To speed up structure solution in such cases it is possible to limit the resolution of the data in Endeavour. In contrast to other structure solution methods, this does not necessarily cause a reduced resolution of the structure model since additional information given by the potential energy is used.

Endeavour can (re-)determine the space group of an arrangement of atoms in a unit cell ("configuration") from a triclinic or other crystal system with low space group symmetry once the structure solution is finalized. The correctness of the space group is confirmed by geometrical analysis of the unit cell contents (arrangement of atoms) resulting from the structure solution calculation. In a first step, the symmetry elements in this atomic arrangement are determined, and, in a second step, the space group is tracked down by comparing the resulting set of symmetry elements to all possible space groups. For this, it uses the symmetry finder as it is implemented in the program Kplot developed by R. Hundt et al. [84,85].

Although Endeavour has first been developed for the solution of crystal structures from X-ray or neutron diffraction data, it can also be applied to ED data. Endeavour

transforms all diffraction data into a powder diffraction-like format for display purposes, although it internally uses 3D diffraction data for structure solution. The adjustment of Endeavour for electron diffraction is firstly reported here as a tool to be systematically applied to 3D ED data. For this, Endeavour uses atomic form factors calculated from X-ray scattering factors by applying the Mott-Bethe formula [86]. The effect of precession is modelled in Endeavour using a formula provided by P. Moeck [87]. Dynamical effects are not considered in the calculation of the reflection intensities.

It should be noted that the combined cost function approach implemented in Endeavour works best if the potential energy includes long-range interactions like the Coulomb forces between differently charged ions. This eliminates (or at least reduces) the danger of getting trapped in some "unphysical" minimum where, for instance, a lot of cations are placed directly in contact to each other, which is rather unlikely to be observed in nature. This "long-range interaction" effect is of course much less prominent in intermetallic or organic molecule compounds. With metals though, there is another effect that facilitates the solution of crystal structures using the Endeavour approach: the dense packing of atoms (especially at increased pressures) leaves little room for alternatives, thus it would be possible to obtain good quality results when solving crystal structures of intermetallic compounds. However, this situation becomes more complicated for organic molecule structures because the covalent bonds between neutral atoms cause the structures to be less dense packed while at the same time miss the long-range directing interactions of Coulomb forces.

Endeavour can also be used to complete a partial structure model, by fixing the positions of known atoms in the crystal structure and have the software search for a limited number of unknown atom positions. This feature was not utilised in the research presented here and it will be explored in future work.

3. Results and Discussion

The obtained structure models for each of the four materials under study are hereunder presented according to the outputs obtained from the three different crystallographic structure solution methods. Datasets acquired with precession have been processed with ADT3D and PETS2 software packages in order to produce two *hkl* files; one in which the reflection intensity is assigned as the maximum of its rocking curve (ADT3D), and another one where the reflection intensity is extracted as the scale factor of the fitting of a double-peaked function to its rocking curve (PETS2). The former will be referred as max-int file while the latter as fit-int file. Both reflection intensity files are independently used to find structure solutions with the different methods. For comparison purposes, the refined unit cell parameters from X-ray data have been used to run the different programs. Nevertheless, unit cell parameters based on 3D ED data are also provided to show that they are closely following the values of X-ray studies.

3.1. $PrBa_2Cu_3O_7$

The reconstruction of the diffraction space from 61 diffraction patterns acquired with 1° of precession allowed to determine the following unit cell parameters in ADT3D: a = 3.81 Å, b = 3.86 Å, c = 11.61 Å, α = 90.2°, β = 90.0° and γ = 90.2°. These values slightly deviate from the ones reported by Bertrand et al. (a = 3.8605 Å, b = 3.9243 Å, c = 11.6993 Å, α = 90°, β = 90.0° and γ = 90°) [60,66] within the typical 1–5% inaccuracy of unit cell parameters determined using ED data [20]. The main crystallographic sections of the reconstructed 3D ED data are shown in Figure 2, which do not show any systematic extinction following the *Pmmm* space group.

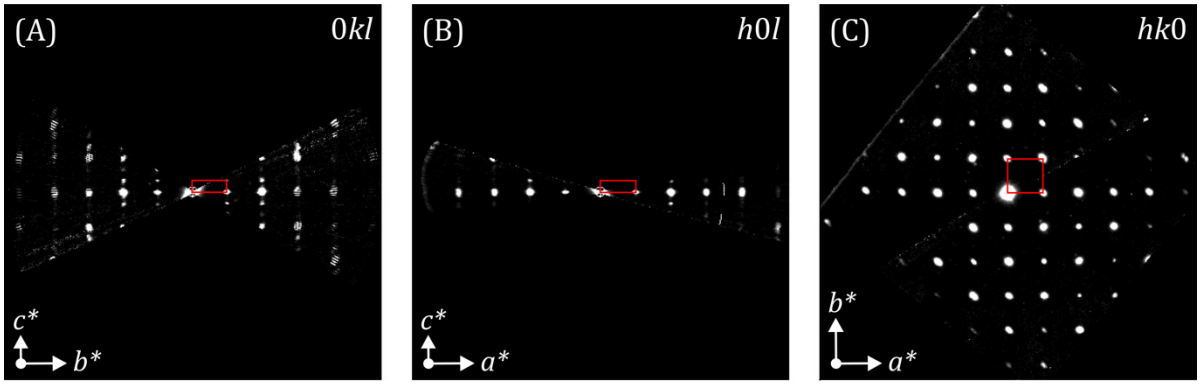

Figure 2. (**A**) 0*kl*, (**B**) *h*0*l* and (**C**) *hk*0 sections of the reconstructed diffraction space of $PrBa_2Cu_3O_7$ from PETS2. The red rectangles represent the projected unit cell along the respective unit cell axes. *a**, *b** and *c** are the reciprocal unit cell axes.

Table 1 shows crystallographic parameters and found atom fractional coordinates of the structure solutions obtained from the different crystallographic methods.

Table 1. Crystallographic experimental parameters of the structure solution of $PrBa_2Cu_3O_7$ and their atomic coordinates obtained by direct methods in SIR2014, charge-flipping in Jana2006 and the global optimization method in Endeavour using the extracted intensities by ADT3D (max-int file) and PETS2 (fit-int file).

	X-ray: Powder [66]	**3D ED with PED**					
		Direct Methods		**Charge-Flipping**		**Global Optimization**	
		ADT3D	**PETS2**	**ADT3D**	**PETS2**	**ADT3D**	**PETS2**
Used Resolution (Å)	-	0.8	0.8	0.8	0.8	-	-
Total/Used [1] Refl. (#)	-	425/95	426/96	425/96	426/97	425	426
Completeness (%)	-	40.4	39.8	41.3	40.2	-	-
R_{int} (%) [2]	-	11.4	13.5	11.4	13.5	11.4	13.5
R(F)/R1(obs) (%) [3]	-	10.7	11.0	37.5	56.6	59.35 [5]	60.89 [5]
RMSD [4]	-	0.123	0.079	0.013	0.104	0.130	0.120
		Atomic fractional coordinates (x, y, z)					
Pr1	0.5 0.5 0.5	0.5 0.5 0.5	0.5 0.5 0.5	0.5 0.5 0.5	0.5 0.5 0.5	0.5 0.5 0.5	0.5 0.5 0.5
Ba1	0.5 0.5 0.1804	0.5 0.5 0.165	0.0 0.0 0.159	0.5 0.5 0.177	0.5 0.5 0.164	0.5 0.5 0.185	0.5 0.5 0.185
Cu1	0.0 0.0 0.0	0.0 0.0 0.0	0.0 0.0 0.0	0.0 0.0 0.0	0.0 0.0 0.0	0.0 0.0 0.0	0.0 0.0 0.0
Cu2	0.0 0.0 0.3515	0.0 0.0 0.293	0.0 0.0 0.336	0.0 0.0 0.349	0.0 0.0 0.320	0.0 0.0 0.359	0.0 0.0 0.359
O1	0.0 0.5 0.0	0.0 0.5 0.0	Not found	Not found	Not found	0.0 0.5 0.0	0.0 0.5 0.0
O2	0.0 0.0 0.168	Not found	Not found	Not found	Not found	0.0 0.0 0.181	0.0 0.0 0.178
O3	0 0.5 0.365	Not found	Not found	Not found	Not found	0.0 0.5 0.391	0 0.5 0.390
O4	0.5 0 0.383	0.5 0.0 0.3655	Not found	Not found	Not found	0.5 0.0 0.391	0.5 0 0.389

[1] *Used reflections refer to symmetrically independent reflections up to the used resolution.* [2] *As given by SIR2014 for ADT3D hkl files and as given by PETS2 for PETS2 hkl files.R(F) as given by SIR2014 for direct methods solutions and R1(obs) as given by Jana.* [3] *2006 calculated from the obtained charge-flipping solutions.* [4] *Calculated in SIR2014 only from the found atoms.* [5] *Calculated by Endeavour software after the global optimization of the structure.*

3.1.1. Direct Methods

The use of the max-int file reported all the metal atoms present in the compound and two of the four symmetrically independent oxygens. Three more ghost atoms are given by the program, but they do not make chemical sense and they are more likely related to termination errors as they appear close to special positions. Although both oxygens are very close to their reference positions, one of the Cu atoms is placed 0.7 Å away from the reference one, which would require further refinements including the two missing oxygens to check if this copper is then properly positioned. When the fit-int file is used for comparison, the four metal atoms are correctly spotted with much better accuracy (up to 0.25 Å) than the result from the max-int file, but oxygen positions could not be found, even with several ghost atoms appearing in the solution. Although the *R(F)* value is quite good in both cases (10.7% and 11.0%, respectively), the low completeness of the dataset (around 40%) limits the capability of the algorithm to correctly identify all atom positions.

3.1.2. Charge-Flipping

The use of both extracted intensity files to run charge-flipping reported similar results to the ones obtained from direct methods. For the max-int file, metal atoms are much better positioned (up to 0.04 Å with respect to the reference), although oxygen positions are not located. In the case of the fit-int file, oxygen positions are still not found, and metal atoms are placed with a maximum difference with respect to the reference structure of 0.4 Å. The *R1(obs)* accounts to 37.5% and 56.6%, respectively, which is quite different to the values obtained in SIR2014 but comes as a result of how the *R* factor is calculated in each software package (SIR2014 also includes ghost atoms in the structure model after finishing the execution of direct methods). More interesting is the difference between the *R1(obs)* of the two obtained models in Jana2006. This points out how the higher displacement of the Cu2 atom highly changes the calculated reflection intensities, increases the difference between calculated and observed reflections and thus pushes up the figure-of-merit, providing a hint that some refinement cycles may bring this atomic position to the correct place. Nevertheless, there are no significant differences between these incomplete models and the ones obtained with direct methods, arguing that the low completeness is also a problem for the charge-flipping algorithm.

3.1.3. Global Optimization Method

Extracted reflection intensities from ADT3D and PETS were individually used to run the global optimization method. Unit cell parameters as reported in the literature [60,66], space group *Pmmm*, chemical moiety formula (Pr1Ba2Cu3O7), number of formula units per unit cell (Z = 1), and oxidation states of the atoms (Ba = +2, Pr = +4, O = −2, Cu = +2) were used as input. As reflection intensities may not be too accurate and the structure has many special positions, the potential energy descriptor was given more weight than the *R* factor (0.95 potential energy vs. 0.05 *R* factor). All individual reflections including the Friedel pairs were used instead of any merging of symmetry equivalent reflections.

For both types of extracted intensities, all atomic coordinates (heavy and light atoms) were successfully determined, and correctness of the structures were measured using the root-mean-square deviation (RMSD) with respect to the X-ray reference structure found in the literature (RMSD 0.130 Å for max-int and RMSD 0.120 Å for fit-int). The *R* values for both structures were very similar (*R* factor for max-int: 59.35%, *R* factor for fit-int: 60.89%). The *Pmmm* space group was also correctly confirmed after the determination of the crystal structure. Maximum position shifts observed for one of the O3 atom was 0.3 Å for both structures (Figure 3). It is also worth to point out that the correct atomic positions were also obtained using equal contribution of potential energy vs. *R* factor for both types of extracted intensities, but for better structural accuracy (low RMSD) the higher weight of the potential energy was used during the final global optimization process.

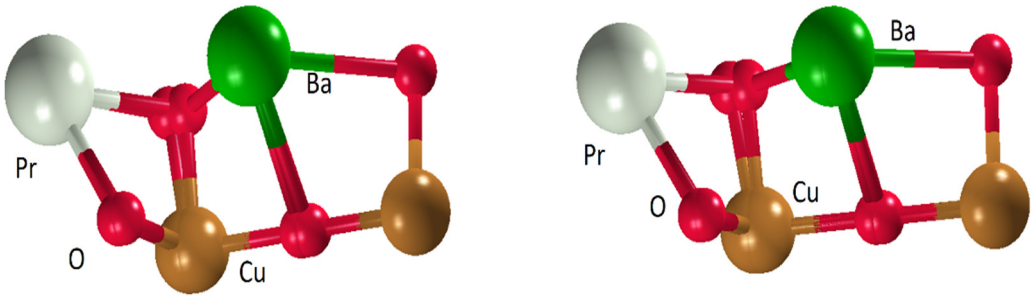

Figure 3. Structural overlays of the X-ray reported structure and the structure obtained by global optimization for the $PrBa_2Cu_3O_7$ compound by using the two differently extracted reflection intensities (**left**: structure from max-int *hkl* file, **right**: structure from fit-int *hkl* file).

3.2. $BaCuO_2$

The reconstruction of the diffraction space from 61 diffraction patterns acquired without the use of precession allowed the determination of the following unit cell parameters in ADT3D: a = 18.20 Å, b = 18.13 Å, c = 18.26 Å, $\alpha = 90.2°$, $\beta = 90.1°$ and $\gamma = 89.3°$. The values are slightly different from the ones reported by Kipka et al. [67] (a = b = c = 18.2700 Å, $\alpha = \beta = \gamma = 90°$) and they are inside the typical 1–5% inaccuracy of unit cell parameters determined using ED data [20]. The 0*kl* and *hhl* crystallographic sections of the reconstructed 3D ED data are shown in Figure 4. The 0*kl* section indicates the reflection condition $h + k = 2n$, while in the *hhl* section the $l = 2n$ is fulfilled, thus matching to the systematic extinctions of the expected $Im\bar{3}m$ space group. It was not possible to collect another dataset with precession from the same sample as beam damage was observed. As there is no data with beam precession, only the max-intensity reflection file was used for structure analysis.

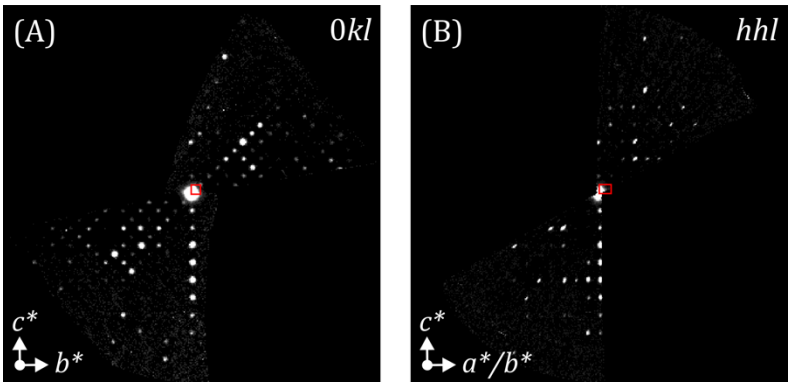

Figure 4. (**A**) 0*kl* and (**B**) *hhl* sections of the reconstructed diffraction space of $BaCu_2$ from PETS2. The red squares represent the projected unit cell along the respective unit cell axes. *a**, *b** and *c** are the reciprocal unit cell axes.

Table 2 shows crystallographic parameters and found atom fractional coordinates of the structure solutions obtained from the different crystallographic methods.

3.2.1. Direct Methods

One of the challenges to obtain structure models from materials like $BaCuO_2$ is to find the positions of partially occupied atoms. In this case, one of the Cu atoms is half-occupied and one of the oxygen atoms is quarter-occupied. Also note that, even if the crystalline structure is highly symmetric, which results in a completeness of 100%, the crystal contains 14 symmetry-independent atoms.

Table 2. Crystallographic experimental parameters of the structure solution of $BaCuO_2$ and their atomic coordinates obtained by direct methods in SIR2014, charge-flipping in Jana2006 and the global optimization method in Endeavour using the extracted intensities by ADT3D (max-int file).

	X-ray: Single-Crystal [67]	**3D ED without PED**		
		Direct Methods	**Charge-Flipping**	**Global Optimization**
Used Resolution (Å)	-	0.87	0.87	-
Total/Used [1] Refl. (#)	-	14719/514	14719/514	14719
Completeness (%)	-	99.4	100	-
R_{int} (%) [2]	-	60.2		60.2
R(F)/R1(obs) (%) [3]	-	15.6	116.1	112.50 [5]
RMSD [4]	-	0.069	0.382	0.698
		Atomic fractional coordinates (x, y, z, a)		
Ba1	0.0 0.151 0.31	0.0 0.1455 0.3051	0.0 0.2916 0.1831	0 0.1396 0.3283
Ba2	0.0 0.364 0.364	0.0 0.3646 0.3646	0.0 0.3475 0.3475	0.137 0.137 0.5
Ba3	0.177 0.177 0.177	0.1785 0.1785 0.1785	0.1335 0.1335 0.1335	0.1710 0.1710 0.1710
Ba4	0.0 0.0 0.0	Not found	Not found	0.0 0.0 0.0
Cu1	0.25 0.15 0.35	0.25 0.1519 0.3481	0.2659 0.1014 0.3827	0.25 0.1445 0.3555
Cu2	0.0 0.125 0.125	0.0 0.1177 0.1177	Not found	0.0 0.1281 0.1281
Cu3	0.206 0.0 0.0	0.2259 0.0 0.0	0.1502 0.0 0.0	-
Cu4	0.43 0.0 0.0 (0.5)	0.4302 0.0 0.0 (1)	0.3701 0.0 0.0 (1)	-
O1	0.072 0.072 0.186	Not found	0.0911 0.0911 0.2380	-
O2	0.144 0.144 0.343	0.1488 0.1488 0.3151	Not found	0.1497 0.1497 0.3283
O3	0.267 0.267 0.085	0.2637 0.2637 0.0897	Not found	-
O4	0.25 0.0 0.5	0.25 0.0 0.5	Not found	0.25 0.0 0.5
O5	0.338 0.0 0.0	Not found	Not found	-
O6	0.0 0.112 0.44 (0.25)	Not found	Not found	-

[1] Used reflections refer to symmetrically independent reflections up to the used resolution. [2] As given by SIR2014 for ADT3D hkl files and as given by PETS2 for PETS2 hkl files. [3] R(F) as given by SIR2014 for direct methods solutions and R1(obs) as given by Jana2006 calculated from the obtained charge-flipping solutions. [4] Calculated in SIR2014 only from the found atoms. [5] Calculated by Endeavour software after the global optimization of the structure.

The retrieval of a structure solution as complete as possible with respect to the reference structure was not an easy task in this case. After some trials of slight changes in composition and resolution used for direct methods, a partial structure model could be obtained. The correct composition of 90 Ba, 90 Cu and 180 O that takes into account the partially occupied elements and a resolution of 0.87 Å were used. In this way, three of the six O positions, three of the four Ba positions and all Cu positions were found in a structure solution given by SIR2014 that contained 15 assigned atoms, five of which were ghost ones.

The *R(F)* for the obtained structure model (including ghost atoms) was 15.6%, but a closer look to how this solution resembles to the reference structure shows a high position deviation for some atoms. The maximum deviation for the found oxygens is about 0.5 Å, 0.4 Å for copper atoms and 0.1 Å for barium ones, a difference that can be confirmed by the high RMSD. The accuracy of the derived model could be improved by some refinement cycles. Furthermore, the high R_{int} value reported by SIR2014 demonstrates how the reflection intensities poorly follow the symmetry relations of the $m\bar{3}m$ Laue class. Low dynamic range of the detector with poor signal-to-noise ratio, beam damage and the possible dynamical effects due to beam precession absence might be associated with the poor data quality, which ultimately gets reflected in the obtained structure model.

3.2.2. Charge-Flipping

After several attempts with Superflip, it was found that a resolution of 0.87 Å and a fixed atomic displacement parameter (ADP) of 2 $Å^2$ allowed to obtain a partial structure solution. In this case, most of the heavy elements were identified but only one of the six oxygens could be identified. However, the majority of the atom positions were deviated between 1.0 Å and 1.4 Å with respect to the reference model. In some cases, atoms had a high displacement close to partially occupied or special positions. For instance, Cu1 should be sitting in a special position, but Superflip assigned its position to a peak near the special one, resulting in a position shift of 1.1 Å. In another case, Cu4 should be a partially occupied atom, but the program assigns a fully occupied atom between its correct position and the close-by and fully occupied oxygen (O5), which leads to a final mismatch of 1.1 Å.

Owing to this highly inaccurate structure model, a final *R1(obs)* of 116.1% is obtained as well as a very high RMSD, which indicates how wrong is the structure with respect to the reference one and shows that, in this example, the structure solution from direct methods is better.

3.2.3. Global Optimization Method

The unit cell parameters as reported in the literature [67], space group $I\,m\bar{3}m$, chemical moiety formula (Ba1 Cu1 O2), number of formula units per unit cell (Z = 90), atom oxidation states (Ba = +2, Cu = +2, O = −2) and extracted reflection intensities were used as input for global optimization. During the structure solution process, no further merging of symmetry equivalent reflections including the Friedel pairs was performed. Due to low quality data and a space group with several special positions and high multiplicity, a higher weight was given to the potential energy descriptor rather than the *R* factor (0.95 potential energy vs. 0.05 *R* factor).

Another challenge for $BaCuO_2$ structure was that there are atomic positions with partial occupation. This feature is currently not yet available for structure solution calculations in Endeavour. For the moment, one has to assume fully occupied positions. Unfortunately, it normally only works if the change of electrostatic potential at a certain position is not overly large. In the case of $BaCuO_2$, there is a half-occupied Cu placed on the special position 12e, so increasing the site occupation factor of this Cu from 0.5 to 1.0 will significantly change the scattering density and hence the reflection intensities. Furthermore, structure solutions with larger unit cell dimensions by global optimization methods take more time to complete. The procedure was sped up by using a restricted dataset that only included reflections up to a 2θ value of 1°, which corresponds to a minimum d-spacing of about 1.44 Å (calculated for a wavelength of 0.0251 Å, the equivalent of electrons accelerated at 200 kV). During the structure solution process some of the ghost atom positions were removed and one of the Cu atom positions were renamed as O atom positions. By increasing the influence of the potential energy and the use of a restricted number of reflection intensities, it was possible to determine all the Ba atomic positions, two Cu atoms and two O atom positions successfully (RMSD 0.698 Å). This final solution took approximately 17 h on a Windows PC with Pentium i3 processors at 3.9 GHz.

3.3. $LiAl_{0.8}Fe_{0.2}(SiO_3)_2$

The reconstruction of the diffraction space from 58 diffraction patterns acquired with 1° of precession allowed the determination of the following unit cell parameters in ADT3D: a = 9.42 Å, b = 8.49 Å, c = 5.28 Å, α = 89.9°, β = 109.9° and γ = 90.0°. Such values are slightly different from the ones reported by Iezzi et al. [65] (a = 9.490 Å, b = 8.426 Å, c = 5.232 Å and β = 110.14°) and they are inside the typical 1–5% error of electron diffraction [20]. The main crystallographic sections of the reconstructed 3D ED data are shown in Figure 5. The 0*kl* crystallographic section exhibits the reflection condition $k = 2n$, while the *h*0*l* fulfils the following condition $h, l = 2n$. Unfortunately, the *hk*0 section does not have enough information to properly assert that systematic extinctions appear when $h + k \neq 2n$, which would confirm the expected $C\,2/c$ space group. When dealing with unknown structures,

the large missing cone of low angular range 3D ED datasets may cause difficulties in the symmetry determination of the crystal under study.

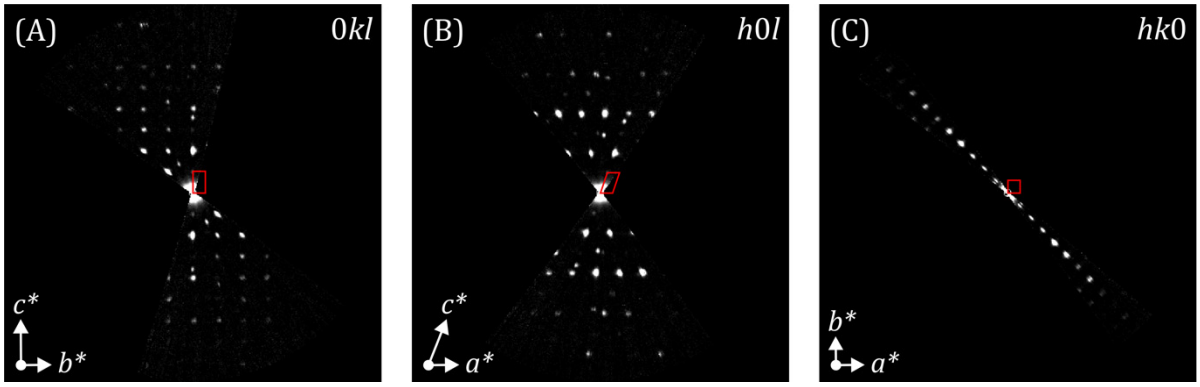

Figure 5. (**A**) 0*kl*, (**B**) *h*0*l* and (**C**) *hk*0 sections of the reconstructed diffraction space of $LiAl_{0.8}Fe_{0.2}(SiO_3)_2$ from PETS2. The red markers represent the projected unit cell along the respective unit cell axes. *a**, *b** and *c** are the reciprocal unit cell axes.

Table 3 shows crystallographic parameters and found atom fractional coordinates of the structure solutions obtained from the different crystallographic methods.

Table 3. Crystallographic experimental parameters of the structure solution of $LiAl_{0.8}Fe_{0.2}(SiO_3)_2$ and their atomic coordinates obtained by direct methods in SIR2014, charge-flipping in Jana2006 and the global optimization method in Endeavour using the extracted intensities by ADT3D (max-int file) and PETS2 (fit-int file).

	X-ray: Single-Crystal [65]	**3D ED with PED**					
		Direct Methods		**Charge-Flipping**		**Global Optimization**	
		ADT3D	**PETS2**	**ADT3D**	**PETS2**	**ADT3D**	**PETS2**
Used Resolution (Å)	-	0.7	0.7	0.7	0.7	-	-
Total/Used [1] Refl. (#)	-	7007/312	1670/322	7007/313	1670/323	7007	1670
Completeness (%)	-	52.7	54.4	53.3	54.8	-	-
R_{int} (%) [2]	-	10.0	19.3	10.0	19.3	10.0	19.3
R(F)/R1(obs) (%) [3]	-	16.5	15.3	71.8	65.8	94.27 [5]	76.32 [5]
RMSD [4]	-	0.026	0.015	0.063	0.020	0.056	0.105
		Atomic fractional coordinates (x, y, z)					
Li1	0.0 0.2746 0.25	Not found	Not found	Not found	Not found	0.0 0.2734 0.25	0.0 0.2609 0.25
Al1/Fe1	0.0 0.9067 0.25	0.0 0.0973 0.75	0.0 0.0981 0.75	0.0 0.0989 0.75	0.0 0.0980 0.75	0.500 0.404 0.25	0.500 0.408 0.25
Si1	0.2941 0.0935 0.2559	0.2926 0.0904 0.2509	0.2948 0.0913 0.2544	0.2922 0.0983 0.2491	0.2901 0.0937 0.2528	0.2956 0.0905 0.2572	0.3003 0.0888 0.2648
O1	0.1096 0.0825 0.1404	0.1012 0.0851 0.1385	0.1064 0.0809 0.1414	0.1157 0.0726 0.1488	0.1091 0.0803 0.1412	0.1172 0.0896 0.1483	0.1141 0.0836 0.1499
O2	0.3647 0.2669 0.3004	0.3737 0.2638 0.3040	0.3682 0.2635 0.3032	0.3800 0.2613 0.2826	0.3732 0.2644 0.3040	0.3589 0.2620 0.2890	0.3619 0.2560 0.2933
O3	0.3565 0.9867 0.0585	0.3546 0.9872 0.0549	0.3569 0.9876 0.0566	Not found	0.3561 0.9870 0.0558	0.3537 −0.014 0.0625	0.3532 −0.013 0.0576

[1] *Used reflections refer to symmetrically independent reflections up to the used resolution.* [2] *As given by SIR2014 for ADT3D hkl files and as given by PETS2 for PETS2 hkl files.* [3] *R(F) as given by SIR2014 for direct methods solutions and R1(obs) as given by Jana2006 calculated from the obtained charge-flipping solutions.* [4] *Calculated in SIR2014 only from the found atoms.* [5] *Calculated by Endeavour software after the global optimization of the structure.*

3.3.1. Direct Methods

The elemental composition provided to direct methods is a key factor for a correct structure solution from ED data because it is associated with the scattering factors that have to be used for the crystal structure determination procedure. However, a composition

of 0.8Al + 0.2Fe, 1.0Al or 1.0Fe in the octahedron position did not significantly change the outcome of this method, thus a fully occupied iron (Fe) position was used. Furthermore, neither direct methods nor charge-flipping are able to give ab initio partially occupied positions, which leaves this structural characterization step to structure refinement.

By using the max-int file or the fit-int file, the whole structure model could be retrieved except for the lithium positions. In both cases, more than 10 ghost atoms are given by SIR2014, but none of them corresponded to the accurate position of lithium. A maximum atom position difference of 0.09 Å is found for one of the oxygens of the structure model related to the max-int file, while a value of 0.04 Å is found for two of the oxygens and iron for the solution of the fit-int file.

The *R(F)* values are 16.5% and 15.3% for the max-int and fit-int structure solutions, respectively. Since both structure models contain the same amount of ghost atoms, it is clear that the difference between them comes from the better accuracy of the model obtained from the fit-int file, also confirmed by the RMSD (0.015 against 0.026).

3.3.2. Charge-Flipping

Charge-flipping was initially performed with the max-int file and a fixed composition for peak search with a fully occupied iron (Fe) in the octahedron position. All atoms were found except for one of the oxygens and the lithium, which Superflip assigned to other peaks from the calculated electrostatic potential. However, one of the correctly spotted oxygens is deviated about 0.2 Å with respect to the reference position. When the fit-int file is instead used, the obtained structure solution is enhanced. All non-lithium atoms are properly located with a maximum deviation of 0.08 Å (corresponding to one of the oxygens) in comparison to the reference model.

The *R1(obs)* is 71.8% for max-int reflections and 65.8% for fit-int reflections. Such high values are obtained mainly because atoms do not have ADP values that properly fit the electrostatic potential, and they would require further refinement steps to improve it. It is also worth to point out how the RMSD jumps for the max-int solution due to the highly deviated oxygen (0.063 against 0.020).

3.3.3. Global Optimization Method

The unit cell parameters as reported in the literature [63], space group *C* 2/*c*, chemical moiety formula (Li1 Al1 Si2 O6), number of formula units per unit cell (Z = 4), atom oxidation states (Li = +1, Al= +3, Si = +4, O = −2) and both extracted reflection intensities were used as input for global optimization. As previous optimization processes, no further merging of symmetry equivalent reflections and Friedel pair reflections was performed. Though the structure has partially occupied Al positions, Endeavour cannot accommodate partial occupancy for the global optimization, so it was assumed that the structure does not contain any Fe atom. Since the ratio of Fe/Al is rather low (1:4) and the electron scattering coefficients of Fe and Al are not highly different, the error introduced by replacing the Fe atoms with Al is limited with respect to the scattering power at the corresponding atomic position. During the initial global optimization, equal weight was given to the Columbic potential energy and the *R* factor, but it turns out that either there are many additional ghost atoms in the structure, or the entire structure solution did not converge to the right model. This could be because of the low quality of the data, thus a new global optimization was performed using higher weight to the potential energy (0.95 potential energy vs. 0.05 *R* factor). With this new weight scheme, structure solution converged, and correct models were obtained from both extracted reflection intensities. Interestingly, Li atom position was also determined, which is always a challenge from direct methods or charge-flipping as Li atoms are mobile in nature with low scattering power. A RMSD of 0.056 Å was obtained for the structure using the max-int reflections, whereas the structure obtained using the fit-int reflections have a RMSD of 0.105 Å (Figure 6). Although the atomic structures are correct, high *R* values (94.27% for max-int reflections and 76.32% for fit-int reflections) were obtained for the final model in the global optimization process.

The latter is potentially related to noise from the high-resolution reflections which has been included during the global optimization process and finally used to calculate the *R* value of the obtained solution from global optimization process. Additionally, *C2/c* symmetry of the solved structure after global optimization process has also been confirmed by the symmetry finder module available in Endeavour.

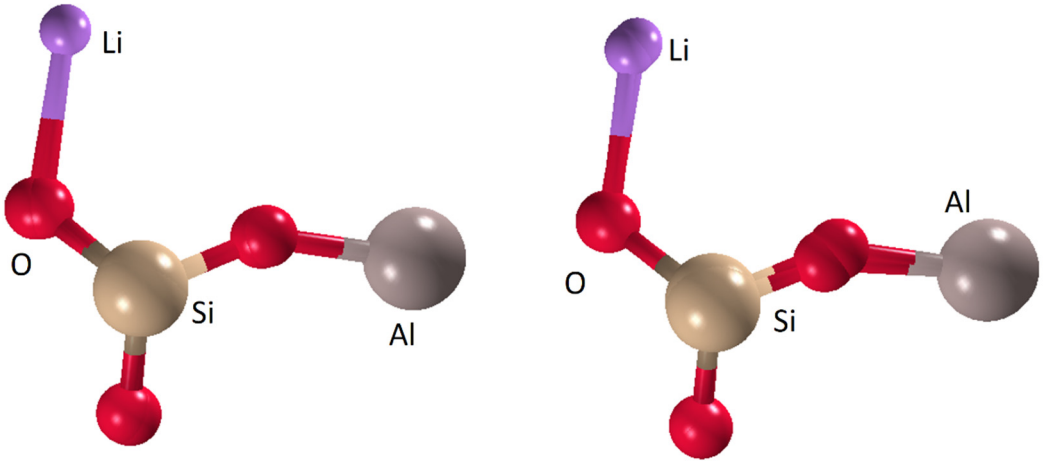

Figure 6. Structural overlays of the X-ray reported structure and the structure obtained by global optimization for the $LiAl_{0.8}Fe_{0.2}(SiO_3)_2$ compound by using the two differently extracted reflection intensities (**left**: structure from the max-int *hkl* file, **right**: structure from fit-int *hkl* file).

3.4. LiAl(SiO$_3$)$_2$

The reconstruction of the diffraction space from 61 diffraction patterns acquired with 1° of precession allowed the determination of the following unit cell parameters in ADT3D: a = 9.97 Å, b = 8.67 Å, c = 5.478 Å, α = 89.5°, β = 111.3° and γ = 90.3°. Such values do not deviate much from the ones reported by Redhammer et al. [63] (a = 9.474 Å, b = 8.390 Å, c = 5.219 Å and β = 110.07°) and they are inside the typical 1–5% inaccuracy of unit cell determination from ED data [19]. The main crystallographic sections of the reconstructed 3D ED data are shown in Figure 7. The 0*kl* section shows that reflections appear when $k = 2n$, the $h, l = 2n$ reflection condition is fulfilled for the *h*0*l* section, and the *hk*0 section exhibits systematic extinctions that belong to the reflection condition $h + k = 2n$, therefore confirming the expected $C2/c$ space group. In comparison to the dataset of $LiAl_{0.8}Fe_{0.2}(SiO_3)_2$, the orientation of the crystal with respect to the geometry of the experimental setup was in such a way that enough information was collected from the main reciprocal sections, which allows here to properly determine the symmetry of the crystal.

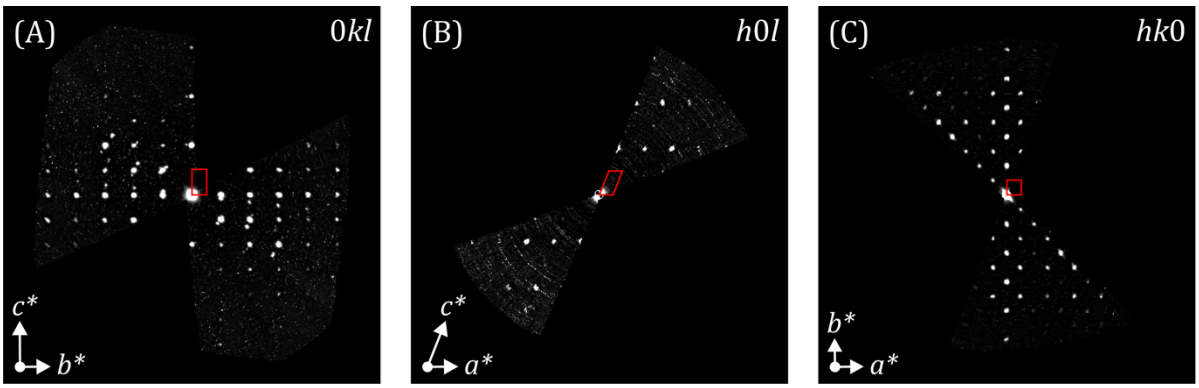

Figure 7. (**A**) 0*kl*, (**B**) *h*0*l* and (**C**) *hk*0 sections of the reconstructed diffraction space of $LiAl(SiO_3)_2$ from PETS2. The red markers represent the projected unit cell along the respective unit cell axes. *a**, *b** and *c** are the reciprocal unit cell axes.

Table 4 shows crystallographic parameters and found atom fractional coordinates of the structure solutions obtained from the different crystallographic methods.

Table 4. Crystallographic experimental parameters of the structure solution of $LiAl(SiO_3)_2$ and their atomic coordinates obtained by direct methods in SIR2014, charge-flipping in Jana2006 and the global optimization method in Endeavour using the extracted intensities by ADT3D (max-int file) and PETS2 (fit-int file).

	X-ray: Single-Crystal [63]	3D ED with PED					
		Direct Methods		Charge-Flipping		Global Optimization	
		ADT3D	PETS2	ADT3D	PETS2	ADT3D	PETS
Used Resolution (Å)	-	0.7	0.7	0.7	0.7	-	-
Total/Used [1] Refl. (#)	-	1597/256	749/261	1597/257	749/262	1597	749
Completeness (%)	-	44.8	45.7	46.7	47.4	-	-
R_{int} (%) [2]	-	11.8	13.1	11.8	13.1	11.8	13.1
R(F)/R1(obs) (%) [3]	-	12.8	9.3	38.0	48.9	46.59 [5]	44.82 [5]
RMSD [4]	-	0.017	0.025	0.024	0.017	0.035	0.027
		Atomic fractional coordinates (x, y, z)					
Li1	0.0 0.2746 0.25	0.0 0.2688 0.25	0.0 0.2791 0.25	Not found	Not found	0.0 0.2615 0.25	0.0 0.2725 0.25
Al1	0.0 0.9067 0.25	0.0 0.9029 0.25	0.0 0.9066 0.25	0.0 0.9065 0.25	0.0 0.9044 0.25	0.500 0.408 0.246	0.500 0.407 0.246
Si1	0.2941 0.0935 0.2559	0.2980 0.0951 0.2555	0.2974 0.0945 0.2517	0.2892 0.0951 0.2630	0.2917 0.0941 0.2565	0.2899 0.0942 0.2690	0.2941 0.0944 0.2720
O1	0.1096 0.0825 0.1404	0.1040 0.0856 0.1378	0.1096 0.0830 0.1400	0.1019 0.0828 0.1420	0.1049 0.0844 0.1430	0.1137 0.0840 0.1310	0.1129 0.0846 0.1250
O2	0.3647 0.2669 0.3004	0.3647 0.2691 0.2972	0.3565 0.2658 0.3073	0.3628 0.2666 0.2999	0.3646 0.2663 0.3014	0.3586 0.2665 0.2980	0.3611 0.2652 0.2960
O3	0.3565 0.9867 0.0585	0.3555 0.9912 0.0598	0.3628 0.9872 0.0469	0.3601 0.9920 0.0579	0.3618 0.9914 0.0598	0.3492 −0.016 0.0697	0.3543 −0.022 0.0621

[1] *Used reflections refer to symmetrically independent reflections up to the used resolution.* [2] *As given by SIR2014 for ADT3D hkl files and as given by PETS2 for PETS2 hkl files.* [3] *R(F) as given by SIR2014 for direct methods solutions and R1(obs) as given by Jana2006 calculated from the obtained charge-flipping solutions.* [4] *Calculated in SIR2014 only from the found atoms.* [5] *Calculated by Endeavour software after the global optimization of the structure.*

3.4.1. Direct Methods

The max-int file was first used to retrieve the structure model. Although twelve ghost atoms were given by SIR2014, silicon, aluminum and oxygen atoms were correctly found with electrostatic potential peaks significantly higher than the remaining atomic positions, and a maximum deviation with respect to the reference structure model of 0.06 Å, which correspond to one of the oxygens. The lithium was spotted to be one of the atoms with much lower potential values and a position difference of 0.05 Å in comparison to the reference one.

The result of the fit-int file is quite similar to the one of max-int file. In this case, the six highest peaks obtained by SIR2014 correspond to the six atoms of the structure model. The software package correctly assigned the element for each atom. A maximum position difference of 0.1 Å is detected for two of the oxygens, while lithium is placed very closed to the reference one (0.04 Å).

The *R(F)* values obtained from both structures (including ghost atoms) are 12.8% and 9.3%, respectively. Here it is interesting to note that the *R(F)* is better for the fit-int file even if the structure model is slightly worse with respect to the reference one. In comparison to the result of $PrBa_2Cu_3O_7$, the low completeness does not seem to be a limiting factor for finding a correct structure solution, and the higher quality of the reflection intensities helps to elucidate a proper crystalline model.

3.4.2. Charge-Flipping

Initially, the max-int file was used to retrieve structure models. After changing the default ADP to 2 $Å^2$ (B_{iso}) and selecting a fixed composition for peak search, a structure

solution with all atoms except lithium could be found with a maximum deviation of 0.08 Å (corresponding to one of the oxygens) with respect to the reference positions. SUPERFLIP assigned the lithium to other maxima of the calculated electrostatic potential but far away from the correct one. This has been also the case for SIR2014 when dealing with the max-int file, but the availability of other ghost atoms in the given structure solutions allowed the possibility to properly locate it.

The extracted results from the fit-int file were not different to the ones obtained with the max-int file, although the default value for the ADP (0 $Å^2$) was kept in this case. A maximum deviation with respect to the reference structure was found to be 0.06 Å for one of the oxygens.

The final *R1(obs)* for these structure models are 38.0% and 48.9%, respectively, and, similar to the results from direct methods, the low completeness doesn't prohibit to properly obtain accurate structure models. One of the differences is that the parameters of SUPERFLIP (method to assign atom positions, ADP value and resolution) had to be tweaked more than in SIR2014 so that the program could correctly interpret and assign the peaks of the electrostatic potential.

3.4.3. Global Optimization Method

The same global optimization process has been followed for $LiAl(SiO_3)_2$ as described previously for $LiAl_{0.8}Fe_{0.2}(SiO_3)_2$. The only difference between these compounds is that for the current structure, $LiAl(SiO_3)_2$, all atom positions are fully occupied. It was also necessary here to set higher weight for the Coulomb potential energy (0.95 potential energy vs. 0.05 *R* factor), otherwise the structure solution did not converge to the right model. In this way, it was also possible to successfully determine all atom positions, including the light Li atom positions for both type of extracted intensity (RMSD of 0.035 Å for the max-int intensity file and RMSD 0.027 Å for the fit-int intensity file) (Figure 8). Interestingly, *R* values for the final structures were much lower in comparison to $LiAl_{0.8}Fe_{0.2}(SiO_3)_2$ (46.59% for max-int *hkl* file and 44.82% for fit-int *hkl* file). The possible difference in *R* values may come due to the better reflection intensities quality obtained using a superior camera, which also allowed a data acquisition procedure in low dose conditions to minimize beam damage. Furthermore, the use of STEM mode for crystal search and data acquisition also facilitates and reduces redundant illumination of targeted crystals, a feature that is essential in order to get suitable data for crystal structure determination of beam sensitive materials such as Li-containing compounds [17,18].

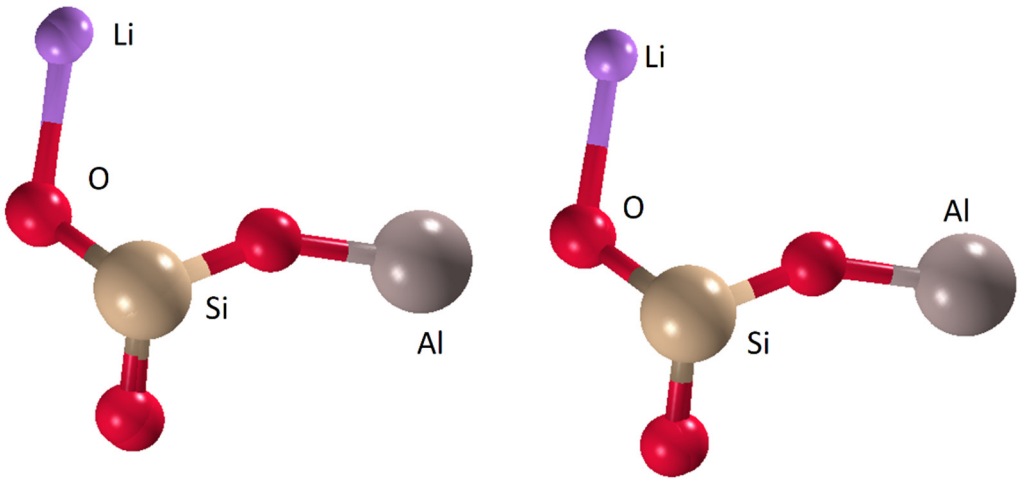

Figure 8. Structural overlays of the X-ray reported structure and the models obtained by global optimization of $LiAl(SiO_3)_2$ by using the differently extracted reflection intensities (**left**: structure from max-int *hkl* file, **right**: structure from fit-int *hkl* file).

4. Conclusions

Four inorganic materials have been studied by means of 3D ED data with different degrees of completeness and quality for crystal structure determination. Each compound was evaluated by three different structure solution algorithms (direct methods, charge-flipping and global optimization), and two different intensity extraction methods were also compared for three of the datasets. Analysis of the structure solution success was given by comparing the models from ED data with the corresponding phases obtained from X-ray diffraction found in the literature.

The global optimization method as implemented in Endeavour successfully found all atom positions for $LiAl_{0.8}Fe_{0.2}(SiO_3)_2$, $LiAl(SiO_3)_2$ and $PrBa_2Cu_3O_7$, including the lithium ones. However, this method is not designed to handle crystal structures with partially occupied atom positions, like $BaCuO_2$, which may lead to spurious atom positions in the structure solution, thus challenges in terms of finding an initial model. Furthermore, structures that have high symmetry and unit cells with at least one long axis become computationally expensive and, at the end, considerably slows down the search for the global optimum.

The results presented here also show that a robust and successful ab initio structure solution by direct methods is possible for beam sensitive Li-bearing compounds even from datasets with low completeness (~45%), provided that the data is acquired in low dose conditions with a higher signal-to-noise electron detector. It has also been observed that in these conditions crystal structure determination from direct methods is slightly more robust than charge-flipping, which may be expected given the statistical foundation of the direct methods algorithm. Another way to improve the chance of a successful structure solution would be to merge different datasets of the same material to push up the completeness, but this was out of the scope in this work and it has been already reported [88,89].

The more challenging dataset analysed here was the case of $BaCuO_2$, where even the heavy atom positions were not successfully determined with any of the tested methods. This could be explained by its occupational disorder, the 3D ED collection without the use of precession and the poor data quality of the detector. One way to increase the chances to retrieve a successful model would be to acquire such data with the use of precession, since it has been demonstrated that the integration of reflections by means of precession helps to minimize dynamical effects [90] thus reflections could follow better the kinematical theory of diffraction from which direct methods, charge-flipping and global optimization are based on. However, these algorithms are not designed to give ab initio partially occupied atoms and it may still require to refine the structure solutions in order to properly describe the material.

The global optimization method can be considered as an alternative crystallographic structure solution method for 3D ED data by adjusting the weighting of the potential energy with respect to the *R* factor. It is important to keep in mind that the primary goal of this method should not be the chase for an extremely low *R* value. Instead, one is looking for a chemically and physically reasonable structure model for which the calculated *R* value is the lowest of all candidate structures (i.e., solutions obtained from multiple Endeavour runs with different seed values). The structure analyses carried out in this work showed that even when the *R* value of a reasonable structure model is around 40–50%, the *R* values of competing solutions are typically still larger (e.g., 70–80% or even more), thus the relatively best *R* value is what one has to look for. However, an *R* value of 40–50% can be reached by a large variety of arbitrary atomic arrangements, but most of them are not reasonable from a physical/chemical point of view. For this reason, the inclusion of the potential energy in the cost function helps to eliminate this large majority of unreasonable structure models. At this point one could even think of completely omitting the diffraction data and optimizing just the potential energy of the system, i.e., to predict the crystal structure. While this is certainly possible in Endeavour, it turns out that in many cases the resulting structure models are still somewhat wrong. They may already be similar to the correct crystal structure, but there are typically still some details missing. The main reason for this is the extremely simple

2-body-function used for the calculation of the potential energy (Coulomb interactions and minimum interatomic distances, as shown in the Supplementary Materials) [91–93]. The addition of the *R* value linked to the experimental diffraction data in the overall cost function helps to drive the model into the right direction, even if reflection intensities deviate from their theoretically expected values. In other words, the use of experimental data enables the bridge from crystal structure prediction to crystal structure determination.

Global optimization methods in general are computationally expensive techniques, therefore their use should be recommended for the edge cases where direct methods or charge-flipping fail to yield a structure. The presented results show how data acquired with older TEMs and detectors can be utilised to successfully obtain structures of inorganic compounds via the application of global optimisation methods. Ultimately, this increases the accessibility of instruments that can be used to collect 3D ED data for crystal structure determination of nanocrystals.

Supplementary Materials: The following supporting information can be downloaded at: https://www.mdpi.com/article/10.3390/sym14112355/s1.

Author Contributions: P.P.D., S.P.-R., A.S.G., A.S., F.K. and H.P. participated in data collection and processing. Conceptualization, S.N., G.I. and I.M.; methodology, I.M., G.I. and M.C.; validation, M.C.; resources, S.N. and I.M.; data curation, G.I.; writing—review and editing, S.N.; funding acquisition, S.N. All authors contributed to the writing and editing of the manuscript. All authors have read and agreed to the published version of the manuscript.

Funding: NanoMEGAS SPRL which acknowledges funding support for this research work from the European Union Seventh Framework Programme under grant agreement 312483–ESTEEM2 (Integrated Infrastructure Initiative-I3). G.I. was supported by the "Fondi Ateneo of the University G. D'Annunzio" and PRIN (2017J277S9_003) project "Time Scales of Solidification in Magmas: Application to Volcanic Eruptions, Silicate Melts, Glasses, Glass-Ceramics." I.M. acknowledges this research was supported by the Hellenic Foundation for Research and Innovation (HFRI) under the 'First Call for HFRI Research Projects to Support Faculty Members and Researchers and the Procurement of High-Cost Research Equipment Grant' (project No. 3051).

Institutional Review Board Statement: Not applicable.

Informed Consent Statement: Not applicable.

Data Availability Statement: Not applicable.

Acknowledgments: NanoMEGAS SPRL would like to thank the laboratory of Electron Microscopy & Microanalysis, School of Natural Sciences, University of Patras, Greece, for support during this study.

Conflicts of Interest: The authors declare no conflict of interest.

References

1. Cowley, J.M. *Electron Diffraction Techniques*; Oxford University Press: Oxford, UK, 1992; Volumes 1 and 2.
2. Dorset, D.L. *Structural Electron Crystallography*; Plenum Press: New York, NY, USA, 1995.
3. Dorset, D.L.; Hauptman, H.A. Direct phase determination for quasi-kinematical electron diffraction intensity data from organic microcrystals. *Ultramicroscopy* **1976**, *1*, 195–201. [CrossRef]
4. Dorset, D.L. Electron crystallography. *Acta Crystallogr. Sect. B Struct. Sci.* **1996**, *52*, 753–769. [CrossRef]
5. Zhou, X.; Hovmöller, S. Electron crystallography: Imaging and single-crystal diffraction from powders. *Acta Crystallogr. Sect. A* **2008**, *64*, 149–160. [CrossRef]
6. Sinkler, W.; Own, C.S.; Marks, L.D. Application of a 2-beam model for improving the structure factors from precession electron diffraction intensities. *Ultramicroscopy* **2007**, *107*, 543–550. [CrossRef] [PubMed]
7. Ciston, J.; Deng, B.; Marks, L.D.; Own, C.S.; Sinkler, W. A quantitative analysis of the cone-angle dependence in precession electron diffraction. *Ultramicroscopy* **2008**, *108*, 514–522. [CrossRef] [PubMed]
8. White, T.A.; Eggeman, A.S.; Midgley, P.A. Is precession electron diffraction kinematical? Part I:: "Phase-scrambling" multislice simulations. *Ultramicroscopy* **2010**, *110*, 763–770. [CrossRef]
9. Palatinus, L.; Jacob, D.; Cuvillier, P.; Klementová, M.; Sinkler, W.; Marks, L.D. Structure refinement from precession electron diffraction data. *Acta Crystallogr. Sect. A* **2013**, *69*, 171–188. [CrossRef]
10. Vincent, R.; Midgley, P.A. Double conical beam-rocking system for measurement of integrated electron diffraction intensities. *Ultramicroscopy* **1994**, *53*, 271–282. [CrossRef]

11. Own, C.S. System Design and Verification of the Precession Electron Diffraction Technique. Ph.D. Thesis, Northwestern University, Evanston, IL, USA, 2005.
12. Nicolopoulos, S.; Weirich, T.E. ELCRYST 2005 proceedings of the electron crystallography school 2005: New frontiers in electron crystallography. *Ultramicroscopy* **2007**, *107*, 431–558.
13. Available online: www.nanomegas.com (accessed on 10 June 2022).
14. Portillo, J.; Rauch, E.F.; Nicolopoulos, S.; Gemmi, M.; Bultreys, D. Precession Electron Diffraction Assisted Orientation Mapping in the Transmission Electron Microscope. *Mater. Sci. Forum* **2010**, *644*, 1–7. [CrossRef]
15. Darbal, A.D.; Narayan, R.D.; Vartuli, C.; Lian, G.; Graham, R.; Shaapur, F.; Nicolopoulos, S.; Weiss, J.K. Automated High Precision Strain Measurement Using Nanobeam Diffraction Coupled with Precession. *Microsc. Microanal.* **2013**, *19*, 702–703. [CrossRef]
16. Hoque, M.M.; Vergara, S.; Das, P.P.; Ugarte, D.; Santiago, U.; Kumara, C.; Whetten, R.L.; Dass, A.; Ponce, A. Structural Analysis of Ligand-Protected Smaller Metallic Nanocrystals by Atomic Pair Distribution Function under Precession Electron Diffraction. *J. Phys. Chem. C* **2019**, *123*, 19894–19902. [CrossRef]
17. Kolb, U.; Gorelik, T.; Kübel, C.; Otten, M.T.; Hubert, D. Towards automated diffraction tomography: Part I—Data acquisition. *Ultramicroscopy* **2007**, *107*, 507–513. [CrossRef]
18. Kolb, U.; Gorelik, T.; Otten, M.T. Towards automated diffraction tomography. Part II—Cell parameter determination. *Ultramicroscopy* **2008**, *108*, 763–772. [CrossRef] [PubMed]
19. Mugnaioli, E.; Gorelik, T.; Kolb, U. "Ab initio" structure solution from electron diffraction data obtained by a combination of automated diffraction tomography and precession technique. *Ultramicroscopy* **2009**, *109*, 758–765. [CrossRef] [PubMed]
20. Kolb, U.; Mugnaioli, E.; Gorelik, T.E. Automated electron diffraction tomography—A new tool for nano crystal structure analysis. *Cryst. Res. Technol.* **2011**, *46*, 542–554. [CrossRef]
21. Kolb, U.; Gorelik, T.; Mugnaioli, E. Automated diffraction tomography combined with electron precession: A new tool for ab initio nanostructure analysis. *MRS Online Proc. Libr.* **2009**, *1184*, 38–50. [CrossRef]
22. Zhang, D.; Oleynikov, P.; Hovmoller, S.; Zou, X. Collecting 3D electron diffraction data by the rotation method. *Z. Krist. Cryst. Mater.* **2010**, *225*, 94–102. [CrossRef]
23. Wan, W.; Sun, J.; Su, J.; Hovmöller, S.; Zou, X. Three-dimensional rotation electron diffraction: Software RED for automated data collection and data processing. *Appl. Crystallogr.* **2013**, *46*, 1863–1873. [CrossRef]
24. Palatinus, L.; Brázda, P.; Jelínek, M.; Hrdá, J.; Steciuk, G.; Klementová, M. Specifics of the data processing of precession electron diffraction tomography data and their implementation in the program PETS2.0. *Acta Crystallogr. Sect. B* **2019**, *75*, 512–522. [CrossRef]
25. Altomare, A.; Burla, M.C.; Camalli, M.; Cascarano, G.L.; Giacovazzo, C.; Guagliardi, A.; Moliterni, A.G.G.; Polidori, G.; Spagna, R. SIR97: A new tool for crystal structure determination and refinement. *J. Appl. Crystallogr.* **1999**, *32*, 115–119. [CrossRef]
26. Altomare, A.; Corriero, N.; Cuocci, C.; Moliterni, A.; Rizzi, R. The hybrid big bang-big crunch method for solving crystal structure from powder diffraction data. *J. Appl. Crystallogr.* **2013**, *46*, 779–787. [CrossRef]
27. Weirich, T.E.; Zou, X.D.; Ramlau, R.; Simon, A.; Cascarano, G.L.; Giacovazzo, C.; Hovmöller, S. Structures of nanometre-size crystals determined from selected-area electron diffraction data. *Acta Crystallogr. Sect. A* **2000**, *56*, 29–35. [CrossRef]
28. Palatinus, L.; Chapuis, G. SUPERFLIP—A computer program for the solution of crystal structures by charge flipping in arbitrary dimensions. *J. Appl. Crystallogr.* **2007**, *40*, 786–790. [CrossRef]
29. Palatinus, L. The charge-flipping algorithm in crystallography. *Acta Crystallogr. Sect. B Struct. Sci. Cryst. Eng. Mater.* **2013**, *69*, 1–16. [CrossRef]
30. Nannenga, B.L.; Shi, D.; Leslie, A.G.W.; Gonen, T. High-resolution structure determination by continuous-rotation data collection in MicroED. *Nat. Methods* **2014**, *11*, 927–930. [CrossRef]
31. Nederlof, I.; van Genderen, E.; Li, Y.-W.; Abrahams, J.P. A Medipix quantum area detector allows rotation electron diffraction data collection from submicrometre three-dimensional protein crystals. *Acta Crystallogr. Sect. D Biol. Crystallogr.* **2013**, *69*, 1223–1230. [CrossRef] [PubMed]
32. Van Genderen, E.; Clabbers, M.T.B.; Das, P.P.; Stewart, A.; Nederlof, I.; Barentsen, K.C.; Portillo, Q.; Pannu, N.S.; Nicolopoulos, S.; Gruene, T.; et al. Ab initio structure determination of nanocrystals of organic pharmaceutical compounds by electron diffraction at room temperature using a Timepix quantum area direct electron detector. *Acta Crystallogr. Sect. A* **2016**, *72*, 236–242.
33. Gemmi, M.; la Placa, M.G.I.; Galanis, A.S.; Rauch, E.F.; Nicolopoulos, S. Fast electron diffraction tomography. *J. Appl. Crystallogr.* **2015**, *48*, 718–727. [CrossRef]
34. Shi, D.; Nannenga, B.L.; Iadanza, M.G.; Gonen, T. Three-dimensional electron crystallography of protein microcrystals. *eLife* **2013**, *2*, e01345. [CrossRef]
35. Clabbers, M.T.B.; van Genderen, E.; Wan, W.; Wiegers, E.L.; Gruene, T.; Abrahams, J.P. Protein structure determination by electron diffraction using a single three-dimensional nanocrystal. *Acta Crystallogr. Sect. D* **2017**, *73*, 738–748. [CrossRef] [PubMed]
36. Clabbers, M.T.B.; Gruene, T.; Parkhurst, J.M.; Abrahams, J.P.; Waterman, D.G. Electron diffraction data processing with DIALS. *Acta Crystallogr. Sect. D Struct. Biol.* **2018**, *74*, 506–518. [CrossRef] [PubMed]
37. Giacovazzo, C.; Monaco, H.L.; Artioli, G.; Viterbo, D.; Milanesio, M.; Gilli, G.; Gilli, P.; Zanotti, G.; Ferraris, G.; Catti, M. *Fundamentals of Crystallography*; Oxford University Press: Oxford, UK, 2011; ISBN 9780199573653.
38. Dorset, D.L. Direct methods and refinement in electron and X-ray crystallography—Diketopiperazine revisited. *Z. Krist.* **2010**, *225*, 86–93. [CrossRef]

39. Palatinus, L. Structure Solution by Charge Flipping. In *Unitin Electron Crystallography and Powder Diffraction*; NATO Science for Peace and Security Series B: Physics and Biophysics; Kolb, U., Shankland, K., Meshi, L., David, W.I.F., Eds.; Springer: Dordrecht, The Netherlands, 2012; ISBN 9789400755796. [CrossRef]
40. Palatinus, L.; Van Der Lee, A. Symmetry determination following structure solution in P1. *J. Appl. Crystallogr.* **2008**, *41*, 975–984.
41. David, W.I.F.; Shankland, K.; van de Streek, J.; Pidcock, E.; Motherwell, W.D.S.; Cole, J.C. DASH: A program for crystal structure determination from powder diffraction data. *J. Appl. Crystallogr.* **2006**, *39*, 910–915. [CrossRef]
42. David, W.I.F.; Shankland, K.; Shankland, K.; Shankland, N. Routine determination of molecular crystal structures from powder diffraction data. *Chem. Commun.* **1998**, *8*, 931–932. [CrossRef]
43. Pagola, S.; Stephens, P.W.; Bohle, D.S.; Kosar, A.D.; Madsen, S.K. The structure of malaria pigment β-haematin. *Nature* **2000**, *404*, 307–310.
44. Favre-Nicolin, V.; Cerny, R. FOX, 'free objects for crystallography': A modular approach to ab initio structure determination from powder diffraction. *J. Appl. Crystallogr.* **2002**, *35*, 734–743. [CrossRef]
45. Černý, R.; Favre-Nicolin, V. Direct space methods of structure determination from powder diffraction: Principles, guidelines and perspectives. *Z. Krist.-Cryst. Mater.* **2007**, *222*, 105–113. [CrossRef]
46. Andreev, Y.G.; MacGlashan, G.S.; Bruce, P.G. Ab initio solution of a complex crystal structure from powder-diffraction data using simulated-annealing method and a high degree of molecular flexibility. *Phys. Rev. B* **1997**, *55*, 12011–12017. [CrossRef]
47. Harris, K.D.M.; Johnston, R.L.; Kariuki, B.M. The Genetic Algorithm: Foundations and Applications in Structure Solution from Powder Diffraction Data. *Acta Crystallogr. A* **1998**, *54*, 632–645. [CrossRef]
48. Shankland, K.; David, W.I.F.; Csoka, T. Crystal structure determination from powder diffraction data by the application of a genetic algorithm. *Z. Krist.-Cryst. Mater.* **1997**, *212*, 550–552. [CrossRef]
49. Deem, M.W.; Newsam, J.M. Framework crystal structure solution by simulated annealing: Test application to known zeolite structures. *J. Am. Chem. Soc.* **1992**, *114*, 7189–7198. [CrossRef]
50. Putz, H.; Schön, J.C.; Jansen, M. Combined method for ab initio structure solution from powder diffraction data. *J. Appl. Crystallogr.* **1999**, *32*, 864–870. [CrossRef]
51. Putz, H.; Brandenburg, K. Endeavour—Structure Solution from Powder Diffraction. Crystal Impact. Available online: https://www.crystalimpact.de/endeavour (accessed on 19 February 2021).
52. Hadermann, J.; Abakumov, A.M.; Tsirlin, A.A.; Filonenko, V.P.; Gonnissen, J.; Tan, H.; Verbeeck, J.; Gemmi, M.; Antipov, E.V.; Rosne, H. Direct space structure solution from precession electron diffraction data: Resolving heavy and light scatterers in $Pb_{13}Mn_9O_{25}$. *Ultramicroscopy* **2010**, *110*, 881–890. [CrossRef]
53. Gorelik, T.; Matveeva, G.; Kolb, U.; Schleuß, T.; Kilbinger, A.F.M.; van de Streek, J.; Bohle, A.; Brunklaus, G. H-bonding schemes of di- and tri-p-benzamides assessed by a combination of electron diffraction, X-ray powder diffraction and solid-state NMR. *CrystEngComm* **2010**, *12*, 1824–1832. [CrossRef]
54. Das, P.P.; Mugnaioli, E.; Nicolopoulos, S.; Tossi, C.; Gemmi, M.; Galanis, A.; Borodi, G.; Pop, M.M. Crystal Structures of Two Important Pharmaceuticals Solved by 3D Precession Electron Diffraction Tomography. *Org. Process Res. Dev.* **2018**, *22*, 1365–1372. [CrossRef]
55. Groom, C.R.; Bruno, I.J.; Lightfoot, M.P.; Ward, S.C. The Cambridge Structural Database. *Acta Crystallogr. Sect. B Struct. Sci. Cryst. Eng. Mater.* **2016**, *72*, 171–179. [CrossRef]
56. Faber, J. A New Relational Database Format for Powder Diffraction, Data Mining and Materials Characterization. *Suppl. J. Ceram. Soc. Jpn.* **2004**, S1434–S1438. [CrossRef]
57. Grazulis, S.; Chateigner, D.; Downs, R.T.; Yokochi, A.T.; Quiros, M.; Lutterotti, L.; Manakova, E.; Butkus, J.; Moeck, P.; Le Bail, A. Crystallography Open Database—An open-access collection of crystal structures. *J. Appl. Crystallogr.* **2009**, *42*, 726–729. [CrossRef]
58. Dill, K.A.; Phillips, A.T.; Rosen, J.B. Molecular Structure Prediction by Global Optimization. In *Developments in Global Optimization*; Bomze, I.M., Csendes, T., Horst, R., Pardalos, P.M., Eds.; Kluwer: Dordrecht, The Netherlands, 1997; pp. 217–234.
59. Calestani, G.; Rizzoli, C. Crystal structure of the $YBa_2Cu_3O_7$ superconductor by single-crystal X-ray diffraction. *Nature* **1987**, *328*, 606–607. [CrossRef]
60. Calamiotou, M.; Gantis, A.; Margiolaki, I.; Palles, D.; Siranidi, E.; Liarokapis, E. Phase separation, microstructure and superconductivity in the $Y_{1-x}Pr_xBa_2Cu_3O_y$ compounds. *J. Phys. Condens. Matter* **2008**, *20*, 395224. [CrossRef]
61. Paulus, E.F.; Miehe, G.; Fuess, H.; Yehia, I.; Löchner, U. The crystal structure of $BaCuO_2$. *J. Solid State Chem.* **1991**, *90*, 17–26. [CrossRef]
62. Kuntzinger, S.; Ghermani, N.E. Electron density distribution and Madelung potential in α-spodumene, $LiAl(SiO_3)_2$, from two-wavelength high-resolution X-ray diffraction data. *Acta Crystallogr. Sect. B* **1999**, *55*, 273–284. [CrossRef]
63. Redhammer, G.J.; Roth, G. Structural variation and crystal chemistry of $LiMe^{3+}Si_2O_6$ clinopyroxenes Me^{3+} = Al, Ga, Cr, V, Fe, Sc and In. *Z. Krist.-Cryst. Mater.* **2004**, *219*, 278–294. [CrossRef]
64. Redhammer, G.J.; Roth, G. Structural changes upon the temperature dependent C2/c → P21/c phase transition in $LiMe^{3+}Si_2O_6$ clinopyroxenes, Me = Cr, Ga, Fe, V, Sc and In. *Z. Krist.-Cryst. Mater.* **2004**, *219*, 585–605. [CrossRef]
65. Iezzi, G.; Bromiley, G.D.; Cavallo, A.; Das, P.P.; Karavassili, F.; Margiolaki, I.; Stewart, A.A.; Tribaudino, M.; Wright, J.P. Solid solution along the synthetic $LiAlSi_2O_6$-$LiFeSi_2O_6$ (spodumene-ferri-spodumene) join: A general picture of solid solutions, bond lengths, lattice strains, steric effects, symmetries, and chemical compositions of Li clinopyroxenes. *Am. Mineral.* **2016**, *101*, 2498–2513. [CrossRef]

66. Bertrand, C.; Galez, P.; Jorda, J.L.; Gladyshevskii, R.E. The Pr ($Ba_{1-x}Pr_x$)$_2$ Cu_3O_{7+d} solid solution. A crystal structure and phase diagram study. *Phys. C Supercond.* **1999**, *321*, 151–161. [CrossRef]
67. Kipka, R.; Müller-Buschbaum, H. Über Oxocuprate, XX Ein Erdalkalioxocuprat(II) mit geschlossenen Baugruppen: $BaCuO_2$/about Oxocuprates, XX Alkaline-earth Oxocuprate(II) with Closed Structural Groups: $BaCuO_2$. *Z. Nat. B* **1977**, *32*, 121–123. [CrossRef]
68. Plana-Ruiz, S. Development & Implementation of an Electron Diffraction Approach for Crystal Structure Analysis—TUprints (TU-Darmstadt.De). Available online: https://www.tesisenred.net/handle/10803/670887#page=1 (accessed on 12 January 2022).
69. Plana-Ruiz, S.; Krysiak, Y.; Portillo, J.; Alig, E.; Estradé, S.; Peiró, F.; Kolb, U. Fast-ADT: A fast and automated electron diffraction tomography setup for structure determination and refinement. *Ultramicroscopy* **2020**, *211*, 112951. [CrossRef]
70. Plana-Ruiz, S.; Portillo, J.; Estradé, S.; Peiró, F.; Kolb, U.; Nicolopoulos, S. Quasi-parallel precession diffraction: Alignment method for scanning transmission electron microscopes. *Ultramicroscopy* **2018**, *193*, 39–51. [CrossRef] [PubMed]
71. Smeets, S.; Wang, B.; Cichocka, M.O.; Ångström, J.; Wan, W. Continuous rotation electron diffraction data for zeolite SSZ-27. *Instamatic Zenodo* **2018**. [CrossRef]
72. Gorelik, T.E.; Stewart, A.A.; Kolb, U. Structure solution with automated electron diffraction tomography data: Different instrumental approaches. *J. Microsc.* **2011**, *244*, 325–331. [CrossRef] [PubMed]
73. Kolb, U.; Krysiak, Y.; Plana-Ruiz, S. Automated electron diffraction tomography—Development and applications. *Acta Crystallogr. Sect. B Struct. Sci. Cryst. Eng. Mater.* **2019**, *75*, 463–474. [CrossRef]
74. Cascarano, G.L.; Giacovazzo, C.; Carrozzini, B. Crystal structure solution via precession electron diffraction data: The BEA algorithm. *Ultramicroscopy* **2010**, *111*, 56–61. [CrossRef]
75. Burla, M.C.; Caliandro, R.; Carrozzini, B.; Cascarano, G.L.; Cuocci, C.; Giacovazzo, C.; Mallamo, M.; Mazzone, A.; Polidori, G. Crystal structure determination and refinement via SIR2014. *J. Appl. Crystallogr.* **2015**, *48*, 306–309. [CrossRef]
76. Petříček, V.; Dušek, M.; Palatinus, L. Crystallographic Computing System JANA2006: General features. *Z. Krist.-Cryst. Mater.* **2014**, *229*, 345–352. [CrossRef]
77. Harris, K.D.M.; Tremayne, M. Crystal Structure Determination from Powder Diffraction Data. *Chem. Mater.* **1996**, *8*, 2554–2570. [CrossRef]
78. Louër, D. Advances in Powder Diffraction Analysis. *Acta Cryst. Sect. A* **1998**, *54*, 922–933. [CrossRef]
79. Kaplow, R.; Rowe, T.A.; Averbach, B.L. Atomic Arrangement in Vitreous Selenium. *Phys. Rev.* **1968**, *168*, 1068–1079. [CrossRef]
80. McGreevy, R.L. 6—Reverse Monte Carlo Methods for Structural Modelling. In *Computer Modeling in Inorganic Crystallography*; Catlow, C.R.A., Ed.; Academic Press: London, UK, 1997; pp. 151–184. [CrossRef]
81. Pareto, V. *Cours d'Économie Politique*; F. Rouge: Laussane, Switzerland, 1896.
82. De Leeuw, S.W.; Perram, J.W.; Smith, E.R. Simulation of electrostatic systems in periodic boundary conditions. I. Lattice sums and dielectric constants. *Proc. R. Soc. A* **1980**, *373*, 27–57. [CrossRef]
83. Kirkpatrick, S.; Gelatt, C.D.; Vecchi, M.P. Optimization by Simulated Annealing. *Science* **1983**, *220*, 671–680. [CrossRef] [PubMed]
84. Hannemann, A.; Hundt, R.; Schoen, J.C.; Jansen, M. A New Algorithm for Space-Group Determination. *J. Appl. Cryst.* **1998**, *31*, 922–928. [CrossRef]
85. Hundt, R.; Schoen, J.C.; Hannemann, A.; Jansen, M. Determination of Symmetries and Idealized Cell Parameters for Simulated Structures. *J. Appl. Cryst.* **1999**, *32*, 413–416. [CrossRef]
86. Prince, E. (Ed.) *International Tables for Crystallography. Vol. C: Mathematical, Physical and Chemical Tables*, 3rd ed.; Kluwer Academic Publishers: Dordrecht, The Netherlands, 2004.
87. Moeck, P.; (Portland State University, Portland, OR, USA). Personal communication, 2008.
88. Ge, M.; Yang, T.; Wang, Y.; Carraro, F.; Liang, W.; Doonan, C.; Falcaro, P.; Zheng, H.; Zou, X.; Huang, Z. On the completeness of three-dimensional electron diffraction data for structural analysis of metal-organic frameworks. *Faraday Discuss.* **2021**, *231*, 66–80. [CrossRef]
89. Wennmacher, J.T.C.; Zaubitzer, C.; Li, T.; Bahk, Y.K.; Wang, J.; van Bokhoven, J.A.; Gruene, T. 3D-structured supports create complete data sets for electron crystallography. *Nat. Commun.* **2019**, *10*, 3316. [CrossRef]
90. Palatinus, L.; Petříček, V.; Corrêa, C.A. Structure refinement using precession electron diffraction tomography and dynamical diffraction: Theory and implementation. *Acta Crystallogr. Sect. A* **2015**, *71*, 235–244. [CrossRef]
91. Momma, K.; Izumi, F. VESTA 3 for three-dimensional visualization of crystal, volumetric and morphology data. *J. Appl. Crystallogr.* **2011**, *44*, 1272–1276. [CrossRef]
92. Brown, I.D. 14—The Bond-Valence Method: An Empirical Approach to Chemical Structure and Bonding. *Ind. Chem. Libr.* **1981**, *2*, 1–30. [CrossRef]
93. Brown, I.D.; Altermatt, D. Bond-valence parameters obtained from a systematic analysis of the Inorganic Crystal Structure Database. *Acta Crystallogr. Sect. B* **1985**, *41*, 244–247. [CrossRef]